



Full Length Article

Impact study of beam losses in TRIUMF's BL4N proton cave and ARIEL tunnel

R.S. Augusto ^{*}, A. Trudel¹, J. Mildenberger¹, K. Ardon, L. Egoriti, M. Brownell, D. Rowbotham

TRIUMF, 4004 Wesbrook Mall, Vancouver BC, V6T 2A3, Canada



ARTICLE INFO

Keywords:
Shielding
Dosimetry
Beam losses
Activation
ARIEL

ABSTRACT

As part of the ARIEL project, currently under construction at TRIUMF, a new proton beam line will be installed to transport up to 100 μA of nominal beam energy 480 MeV protons from the main cyclotron extraction port to an isotope separator on-line (ISOL) proton target station. This new beam line, approximately 80 m long, designated beam line 4-North (BL4N), will connect the cyclotron to the ARIEL facility via a tunnel. The proton beam line is designed for beam losses lower than 1 nA m^{-1} and will feature a collimator to remove the beam halo produced by large-angle scattering in the cyclotron extraction foil.

The tunnel will be shared with an electron beam line with its own specific requirements for beam loss mitigation and machine protection, leading to another ISOL electron target station. The electron beam is generated by an e-linac with capacity for 500 kW beam power operation, but is ultimately expected to operate at 100 kW with losses not exceeding 20 nA m^{-1} . After an initial stage of operation at 25 MeV the beam energy will be upgraded to 50 MeV.

In this work, the effect of the beam losses, both chronic and catastrophic, in the tunnel and adjacent areas were studied. The FLUKA particle transport and interaction code was employed to estimate the impact of the combined proton and electron beam losses to the shielding, including as well the reflection of radiation from the target stations into the tunnel during ARIEL operation. This analysis resulted into a better assessment of the damage to equipment in the tunnel and the impact on maintenance due to activation of elements of the beam line. Maximum credible accidental scenarios were also detailed to validate the shielding configuration and the safety systems location.

1. Introduction

1.1. The ARIEL facility

The 520 MeV cyclotron is the main driver of several science programs at TRIUMF and, once BL4N becomes operational, it will enable a fourth proton beam to be extracted in parallel [1,2]. This fourth beam, with approximately 500 MeV and maximum intensity of 100 μA , will be used for rare isotope beam production in the future ARIEL facility, in one of its two target stations [3]. The other target station will operate with an electron beam from the e-linac, initially at 100 kW and 25 MeV, but with capacity for 50 MeV and 500 kW beam power operation [4]. Presently TRIUMF is licensed by the Canadian Nuclear Safety Commission to operate the e-linac up to 40 MeV.

Both the proton and electron beam lines connect to the ARIEL facility via a tunnel [5], from the proton cave and electron hall (E-HALL), respectively (see Fig. 1).

Throughout most of the tunnel the proton beam line runs above (about 1 m) of the electron beam line, the latter runs closer to the floor and only rises to the same elevation of the proton beam line

before entering the Target Pit. Their paths can be seen in Fig. 2. Since these beam lines will operate simultaneously, their functional compatibility is a main requirement. Thus, the beam losses' output from both beam lines were combined to allow for a more accurate estimate of equipment deterioration or quantify the activation and its impact on maintenance activities.

1.2. Source terms

In the tunnel, during regular operation, there are two main radiation sources:

- chronic beam losses – 0.5 W m^{-1} for protons and 1 W m^{-1} for electrons. The BL4N is designed for low beam losses at a rate of less than 1 nA m^{-1} whereas the electron beam line will have variable losses depending on the beam energy. Depending on the latter the rate of beam loss will range from $20\text{--}30 \text{ nA m}^{-1}$, with beam loss monitors enforcing a limit of 1 W m^{-1} [5–7].
- reflected shine from ARIEL target stations — which can become dominant nearer to the northernmost sections of the tunnel. To

* Correspondence to: Radiological Control Division, Brookhaven National Laboratory, Upton, NY 11973-5000, USA.
E-mail address: rdossanto@bnl.gov (R.S. Augusto).

¹ Retired.

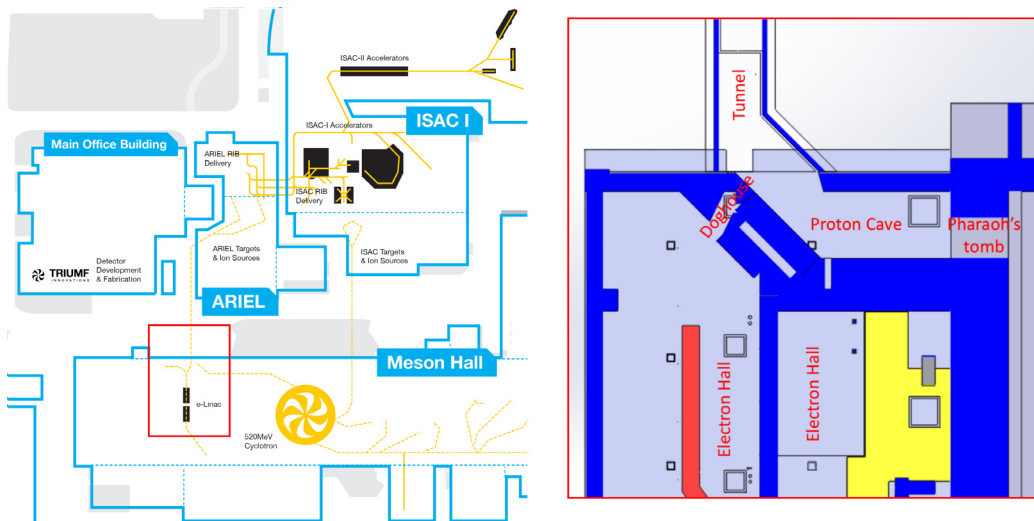


Fig. 1. On the left panel — the schematic view of TRIUMF beamlines network and some of its buildings at ground level. On the right panel — a detail of the underground infrastructure (~6 m below the surface) that will host the BL4N and e-linac beam lines, eventually connecting to the ARIEL tunnel.
Source: Adapted from the TRIUMF website: www.triumf.ca.

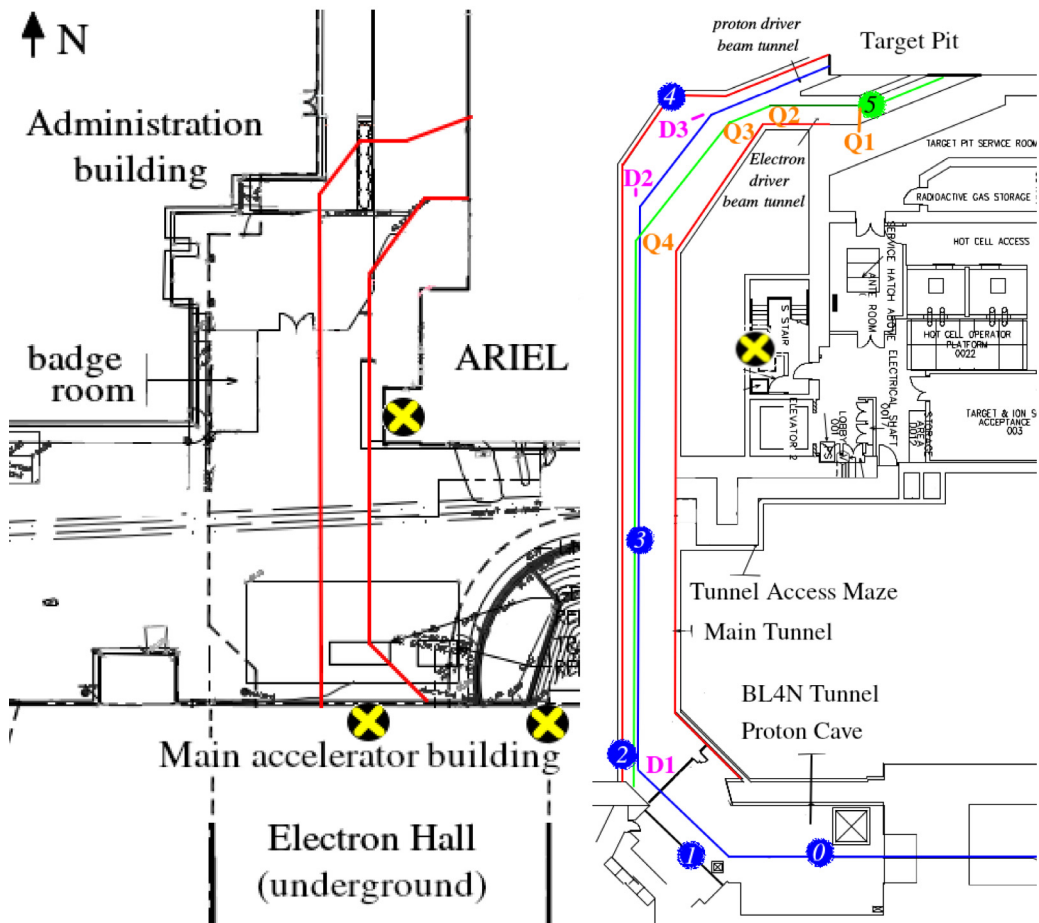


Fig. 2. Left — The outline of the ARIEL tunnel hosting the BL4N at ground level is delimited in red. Right — Underground view showing the ARIEL tunnel and its connections to the ARIEL facility, the main cyclotron and the electron hall. The proton and electron beam lines are highlighted in blue and green, respectively. In the latter, the dark green path denotes a vertical rise in the beam line elevation. The numbered nodes denote the catastrophic beam losses' locations as studied in this work. The "D" and "Q" refer to some of the magnets along the proton and electron beam lines, respectively, in which absorbed dose rates were quantified. The locations of radiation critical safety monitors are marked with yellow-black crosses.

assess the impact of this shine, it was assumed maximum intensity operation using standard uranium carbide targets [8,9]. Thus, the proton beam irradiation parameters consisted of 500 MeV protons at 100 μA . Conversely, 50 MeV and 10 mA were used in the electron station.

In addition to the chronic scenarios above mentioned, six catastrophic beam losses were also considered. The locations of the latter are shown in Fig. 2 and they were selected with the maximum impact on both shielding and occupancy as chief criteria. Due to the penetrative nature of its radiation, these catastrophic cases consisted of proton losses, the exception being one full electron beam loss directly affecting a relevant zone of the ARIEL facility. Proton beams were considered with 500 MeV and 100 μA whereas the electron beam case assumed a 50 MeV beam at 10 mA.

Two maintenance scenarios were also considered: shine from a full beam loss in the main cyclotron spilling into the proton cave (near “0” in Fig. 2) while there is human presence in the tunnel; and the residual dose rate accrued at different times after end of bombardment (EOB) by personnel during routine access.

2. Materials

2.1. Safety requirements

2.1.1. Human occupancy impact

At TRIUMF, workers are identified as Nuclear Energy Workers (NEWs) if there is a reasonable probability of receiving an occupational dose greater than 1 mSv per year. Many workers at TRIUMF do not meet this criterion and thus are classified as non-NEWs. Radiation exposures to NEWs and non-NEWs are monitored to ensure compliance with the Canadian Nuclear Safety Commission’s regulatory dose limits and to maintain radiation doses ALARA. The NEW annual regulatory effective dose limit is 50 mSv (maximum 100 mSv over a five year period) and 1 mSv for a non-NEW.

The main safety requirement is to ensure that dose rate to personnel remains within regulatory limits inside the ARIEL building while, above the tunnel in the zone depicted in Fig. 2, the goal is to maintain dose rates indistinguishable from natural background during normal operation. In the ARIEL facility, the ambient equivalent dose rates are limited to 1 and 10 $\mu\text{Sv h}^{-1}$ for high and low occupancy areas, respectively. The latter limit can be extended to 100 $\mu\text{Sv h}^{-1}$ via administrative controls but above it an exclusion zone is enforced.

It is expected that, after the yearly shutdown, access to the tunnel is allowed. In this case, the main source of radiation to personnel is the residual dose from the beam line components and tunnel walls due to activation, except for the zones closer to the ARIEL target stations where the shine from the stations dominate [9]. During unplanned maintenance scenarios, when personnel accesses to the tunnel are allowed while the main cyclotron is operating, the most significant danger is that of an accidental full beam loss inside the main cyclotron which produces a shower into the BL4N. Besides its original purpose of removing the beam halo [6], the shielded collimator is expected to block the radiation to such extent that most, if not all, of the tunnel remains protected in the event of a full beam loss originating in the main cyclotron. The design of the collimator shielding, covering the whole width of the Proton Cave, primarily limits shine but also activated air from circulating through the tunnel. It ensures as well that there is no personnel access upstream of the collimator via the tunnel.

In the present operational model, chronic beam losses are effectively attenuated by the tunnel shielding design, which consists of the tunnel concrete walls and a soil layer of over 4 m up to the surface. The connection between the tunnel and the ARIEL facility is via a maze visible in Fig. 2, which prevents direct shine from reaching the hot cell area in the ARIEL facility [9]. The proton cave is shielded above to the e-HALL roof with blocks of concrete totaling approximately 4 m, leading

to the main accelerator building. Between the tunnel and the e-HALL e-linac area, radiation is attenuated by a vertical maze (denoted doghouse in Fig. 1) and a combination of steel and concrete blocks.

As for the catastrophic beam losses, these have the potential to affect zones where human presence is allowed, both inside the ARIEL facility as well as at the ground surface and in the e-HALL (note that the latter scenario is only relevant during proton beam extraction, and while the e-linac is not operating). In the event of a catastrophic beam loss, shielding should be designed so that the ambient dose rates in zones where human occupation is possible do not exceed 50 mSv h^{-1} [10]. Thus, a promptly detected full beam loss would not result in integrated exposures in excess of a couple of μSv .

2.1.2. Safety systems

Besides the machine protection system or beam loss monitors that will be placed inside the tunnel, several safety critical monitors will be installed outside of shielding. The latter are safety systems that provide an additional layer of protection and consist of both neutron and gamma radiation detectors and monitors. These out-of-shielding network of radiation safety monitors, partially visible in Fig. 2, will trip the beam when neutron dose rates greater than 1 mSv h^{-1} in the vicinity of the tunnel are detected. Therefore, these are best located where hotspots are deemed likely.

The machine protection safety system is designed to shut down the beam within 100 ms of measuring an excursion [7]. This is a stricter requirement than the off the shelf safety monitors, which trip the beam within 250 ms after a safety critical monitor alarm level is surpassed [11]. This includes the time to detect plus time to shutdown, or 100 ms to shutdown after detection.

2.1.3. Equipment damage

It is expected that over the course of 30 years, the envisaged lifetime of the ARIEL facility, some equipment and components may fail due to radiation damage. Support cabling materials such as plastic piping tubes are examples of services that can be affected by radiation, and thus their selection aimed for at least for 12 years of operation. However, they will be inspected annually and likely replaced before 10 years of usage, ideally during a long shutdown.

On the other hand, some critical beam line elements such as cables and magnet insulators are much more difficult to replace and their malfunction can severely impact the ARIEL duty cycle. Other important elements are the machine protection systems and beam diagnostics. The latter will be particularly useful near the target stations (proton and electron driver beam tunnels in Fig. 2). However, in these locations radiation fields can be relatively high, potentially shortening their anticipated lifetime. Therefore, it is important to assess radiation fields and damage beforehand so that either radiation hard material and equipment can be deployed preventively.

2.2. Simulation details

The beam losses studies were performed with the Monte Carlo particle transport and interaction code FLUKA (version 2021.0) [12,13]. In addition to the ARIEL facility, the tunnel, electron hall and proton cave geometries were also reproduced (see Fig. 3) in order to more accurately assess the impact outside of the shielding.

Despite its low height of 2.7 m and width of ~3 m, the space in the tunnel contains various support and structural elements. However, for simplicity, the beam lines were modeled featuring only the beam pipe and main magnets. This can be also considered conservative from the standpoint of the prompt radiation scenarios driving the shielding design. The proton beam line runs at 1.4 m above the tunnel floor whereas the electron beam line runs 45 cm above the tunnel floor, rising to the same level of the proton beam line after the tunnel bifurcation and before entering the Target Pit as indicated in Fig. 2.

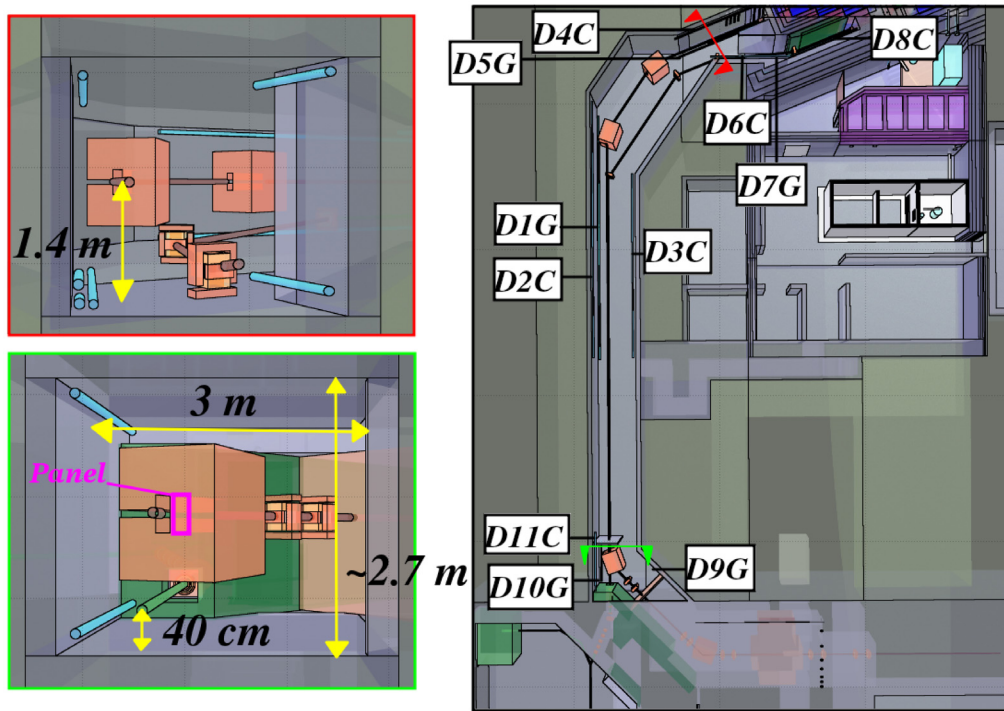


Fig. 3. On the right panel the tunnel is seen in flair [14] geoviewer with the 11 detectors' location highlighted. The "C" and "G" indicates whether the detector is placed at ceiling or ground level, respectively. Two sections, denoted by the red and green arrows, are shown on the left panel, depicting the elevations of the beam lines and the tunnel dimensions. The approximate location and outline of one of the dipole's detector panel is indicated in pink while some of the other detectors are visible in blue.

Ambient dose equivalent maps were scored [15] in the tunnel and adjacent areas, as well as fluences of gamma, neutron and electron radiation. The binning unit consists of cubes with approximately 13 cm side. Several detectors were included in key locations visible in Fig. 3 to estimate material deterioration via the tally of absorbed dose and neutron fluxes, thus providing guidance for service and monitoring placement, respectively.

The FLUKA simulations used PRECISIOn defaults, with transport down to 10 keV for electrons and 5 keV for photons. The proton beam simulations were performed linking the relativistic quantum molecular dynamic model to reproduce both secondary hadron production and residual nuclei distributions [16]. As for electron irradiations, PHOTONUC and ELECTNUC were employed with LAM-BIAS to better account for the photon and electron induced nuclear reactions. In particular, with LAM-BIAS the interaction length for nuclear inelastic interactions of all particles (INEALL) was multiplied by a factor of 0.01. Coalescence and heavy fragment Evaporation were employed to allow for a proper assessment of activation and residual dose rates.

For calculations reflecting post-EOB operation it was required for the simulations to have RADDECAY with Activation enabled. Also, several IRRPROFI cards were used to reproduce the equivalent of ten years of beam time. Scoring was performed combining multiple DCYSCORE and DCYTIMES cards, assigning detectors to the respective times after EOB.

A user importance biasing was assigned via a dedicated usimbs.f user-routine, increasing the importance values of gammas and neutrons through spherical layers centered at the radiation source origin. For each simulation the number of layers, their radii, and common origin, were adjusted according to the source term and surrounding shielding. The importance biasing factor was kept to 2 and large empty rooms and volumes were excluded from the biasing "action range" to prevent the computation time explosion.

2.3. Simulation scenarios

The following scenarios were considered in this work:

- A — Six catastrophic beam losses, representing maximum credible incidents;
- B — Chronic beam losses from both beam lines as specified earlier in Section 1, and also accounting for the shine reflected into the tunnel from both target stations, with regular irradiation parameters;
- C — Personnel entrance into the tunnel at different times post-EOB for maintenance;
- D — Personnel presence in the tunnel when a full loss from the main cyclotron occurs.

Catastrophic beam losses

Catastrophic beam losses were simulated as either point or stray beam losses in the tunnel, aiming for maximum impact in areas of possible human presence. Five out of the six catastrophic events were proton beam losses given that the shielding was seen to be more permeable to fast neutrons. The cases are detailed below:

0. reproduces a total loss in the collimator shielding, with maximal impact to both the E-HALL and main accelerator building, through the concrete shielding;
1. details a full beam loss downstream of the collimator, affecting more directly the E-HALL, and to a less extent the main accelerator building;
2. represents a beam loss in the lateral walls of the tunnel due to a magnet malfunction, consequently leading to radiation propagating throughout the soil up to the ground surface;
3. illustrative of a major loss in the beam pipe resulting from beam miss-steering upstream, causing shine to leak upwards to both the ground level and to the ARIEL facility;
4. same as 2, but having the magnet defectively sending the beam to a weaker spot of the shielding instead;
5. consists of a full power (500 kW) electron beam loss impinging onto a magnet of the tunnel before entering the target station, potentially leading to shine towards human occupied zones.

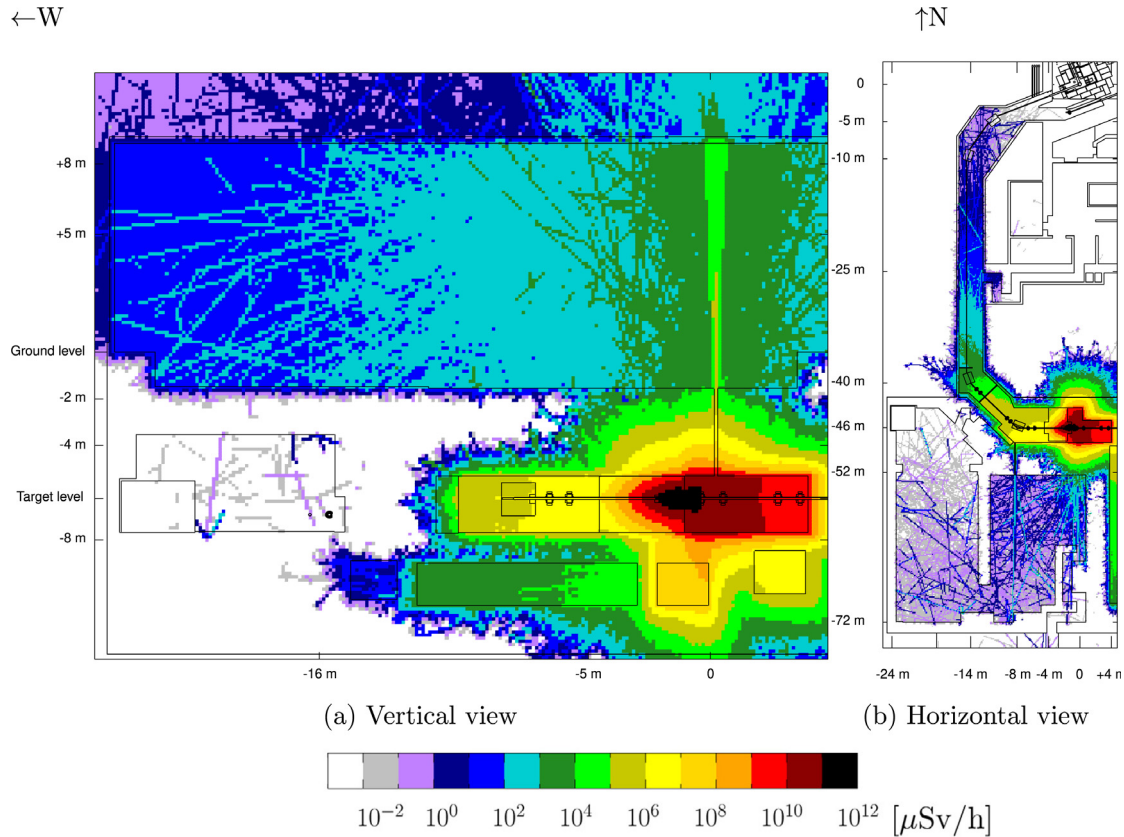


Fig. 4. Ambient dose rates, in $\mu\text{Sv h}^{-1}$, averaged over the tunnel dimensions, seen vertically (a) and horizontally (b) coming from the accidental beam loss into the collimator (case 0).

To provide a result already embedded with a safety factor, each of the above mentioned proton irradiation cases were scaled by a factor of three, except for the electron beam irradiation case since 500 kW is already an unlikely scenario with an implicit safety factor of five. The safety factor of three used in proton calculations is meant to capture uncertainties associated with the FLUKA code, the simulation geometry model and also provide contingency for eventual modifications of the as-built model. Furthermore, in every calculation it was confirmed that where the highest radiation values are scored outside of shielding the statistical errors were kept within a limit of 10%.

Chronic beam losses

Chronic beam losses were reproduced using an annular beam with a smooth divergence, so that energy deposition occurs gradually along the beam line. These losses were defined conservatively as 1 and 20 nA m^{-1} , for proton and electron beam operation respectively. Note that, while chronic losses are more prominent in specific locations (e.g. bending points) rather than constantly along the beam line, the use of a relatively conservative beam loss rate allows for an average assessment of the radiological impact in the tunnel.

As mentioned, the proton beam losses were the most penetrating, but with a relatively low intensity compared to electron beam losses, which were characterized by intense *bremstrahlung* radiation that is strongly forward projected. The impact of the latter was essentially restricted to the tunnel, contrasting with the proton losses. The contribution of the reflected shine originating in the target stations was scored and combined with the chronic beam losses data results in ambient dose rate maps. The cumulative effect of the target stations results in an increase of radiation in the northernmost zone of the tunnel, which is likely to be the worst case scenario for the magnets and also other equipment in the area (e.g. beam diagnostics).

Eleven water detectors, depicted in Fig. 3, were placed throughout the tunnel above the floor or just beneath the ceiling, to assess the

absorbed dose rate at these locations. Furthermore, the energy deposited in some of the dipoles and quadrupoles, denoted in Fig. 2, was also used to estimate dose levels in the magnets' insulation material and explore mitigation measures (e.g. limit the dose contribution from the target stations' reflected shine). Due to the dipole's yoke potential self-shielding and subsequent distortion of the radiation distribution, energy deposition was scored in two panel-shaped detectors attached to the upstream and downstream face of each dipole (see Fig. 3 for the illustration of one of these detectors in the upstream face of the dipole). Absorbed dose rates were also scored in the tunnel to quantify their variation at 90° from the beam lines. Moreover, the fluences of photons, neutrons and electrons were also obtained to disentangle the contribution of different radiation types.

In order to assess the impact of the neutron radiation from the target stations and the beam losses to the diagnostics and electronics in the tunnel, the neutron fluence energy spectra were calculated separately, in two directions – entering the tunnel and towards the target stations, respectively – at the boundary corresponding to the top left panel in Fig. 3.

Personnel access scenarios

Personnel exposure to residual radiation during maintenance was assessed at 1 day, 1 week and 1 month post-EOB. A 10-year operation time was simulated to generate a representative source term. The latter consisted of the residual dose rates originating in the activated elements in the tunnel due to chronic beam losses and the reflected radiation from the target stations during standard operation, merged.

The assumption that shine from a cyclotron's full beam loss can spill into the proton cave while personnel is accessing the tunnel is a very conservative incident. Note that in such maintenance scenario, neither the proton nor the electron beams are extracted from the cyclotron vault or E-HALL into the tunnel, therefore the use of a full proton beam

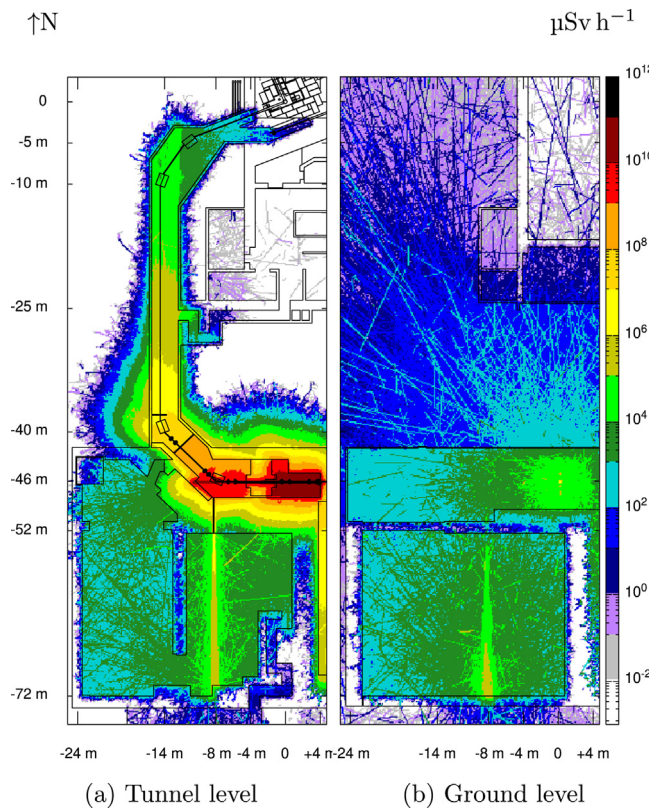


Fig. 5. Ambient dose rates for case 1, in $\mu\text{Sv h}^{-1}$, averaged over the tunnel height (a) and 2 m above ground level (b).

loss upstream of the collimator is conservative. The purpose of this simulation was to demonstrate the capacity of the collimator shielding to effectively attenuate the forward projected shine in the proton cave that otherwise could propagate throughout the tunnel.

3. Results

3.1. Catastrophic losses

Case 0 – a full beam loss into the collimator from a stray proton beam — Fig. 4.

Case 1 – catastrophic event due to the malfunction of the first magnetic dipole, downstream of the collimator, impinging on the shielding protecting the E-HALL — Fig. 5.

Case 2 – dipole magnetic failure, leading to full beam loss into the tunnel lateral wall — Fig. 6.

Case 3 – full beam loss, into the beam line pipe, just upstream of the tunnel maze — Fig. 7.

Case 4 – partial failure of a dipole resulting into a misdeflected beam impinging into the north wall of the tunnel — Fig. 8.

Case 5 – electron beam impinging into a quadrupole vertically at an angle of 45° — Fig. 9.

The Ambient dose rates at ground level above the tunnel are shown in Fig. 10. These were scored along the length of the tunnel in steps of approximately 50 cm and averaged over a width and height of 1 m above ground level and centered at the proton beam line.

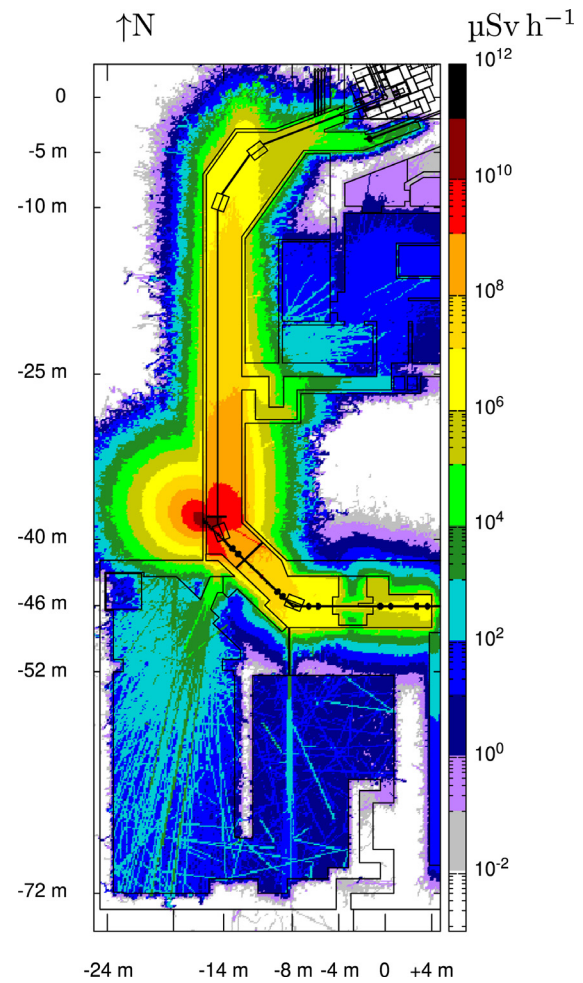


Fig. 6. Ambient dose rates, in $\mu\text{Sv h}^{-1}$, averaged over the tunnel height as mentioned in catastrophic case 2.

3.2. Chronic losses

Chronic beam losses into the tunnel, accounting also for the reflected shine from the target stations, are depicted in Fig. 11. The chronic losses' radiation fluence and absorbed dose rate originating in each of the beam lines is shown in Fig. 12.

Neutron fluence lethargy spectra in the tunnel during regular operation, scored at the bifurcation both exiting and entering the target stations is shown in Fig. 13.

Radiation induced damage to the 11 detectors in the tunnel (see Fig. 3) during regular operation was estimated via the yearly average absorbed dose (\bar{D}) and is shown in Table 1. Moreover, the average distance d between the detector and each beam line was also detailed. The annual average absorbed dose in the quadrupoles and dipoles indicated in Fig. 2 was also quantified. For each dipole the absorbed dose was calculated in a pair of detectors attached to the upstream and downstream face of the yoke and adjacent to the beam line as shown in Fig. 3. The detectors consist of 1 cm thick CTD-101K [17] panels with 20 cm width and 40 cm height.

3.3. Personnel access scenarios

The residual dose rates during maintenance at different times post EOB in the tunnel are shown in Fig. 14.

An accidental full beam loss originating from the main cyclotron during maintenance in the tunnel is depicted in Fig. 15.

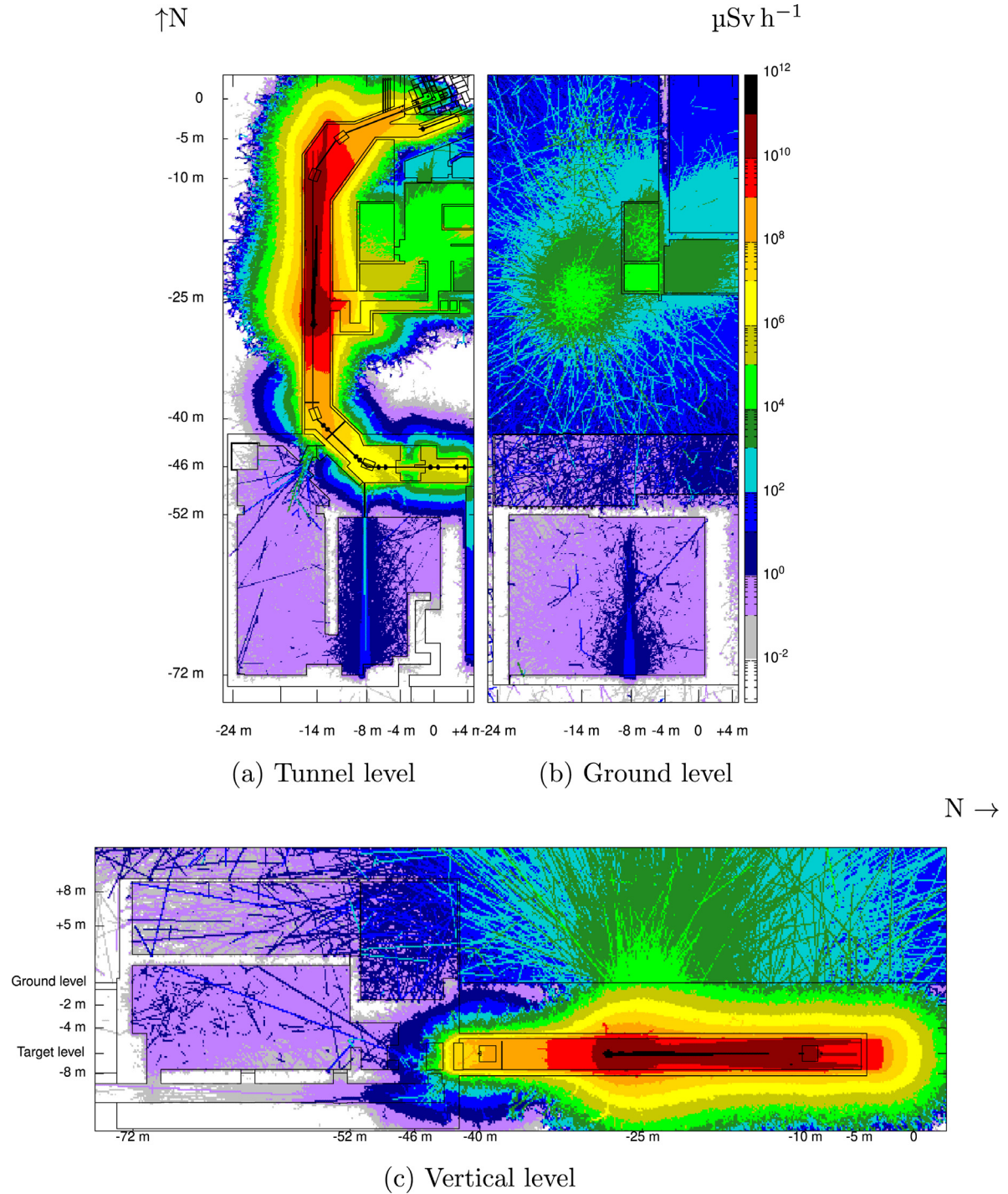


Fig. 7. Ambient dose rates for case 3, in $\mu\text{Sv h}^{-1}$, averaged over the tunnel height (a) and 2 m above ground level (b). The result in the lower panel (c) depicts a vertical view averaged over the tunnel width.

4. Discussion

Catastrophic beam losses

The catastrophic beam losses results in Fig. 4-a reveal major leaks to the main accelerator building through the vertical chases leading to the top of the shielding, as a result of a full loss into the collimator shielding. Consequently, most chases will be back-filled and the essential services will be shielded. Except for the leakage at service chases, the radiation is approximately 1 mSv h^{-1} . In the E-HALL, the results of 4-b do not evidence any major issue and are within the 50 mSv h^{-1} limit

(note the safety factor of three). Such ambient dose rates will be only observed for fractions of a second due to the prompt action of machine protection systems, beam loss or radiation safety monitors.

As for the second case, whose results are depicted in Fig. 5, they illustrate how the radiation reaches the E-HALL via a 15-cm-wide empty service chase in the shielding – note the leak towards the South in $[-8:-52]$ in Fig. 5-a – and still penetrates into the main accelerator building through the aforementioned vertical openings (see Fig. 5-b). Due to the major leak to the E-HALL, the opening will have to be shielded.

Case 2, illustrated in Fig. 6, sees the beam directed towards the tunnel lateral wall and into the soil. Since the soil was modeled with

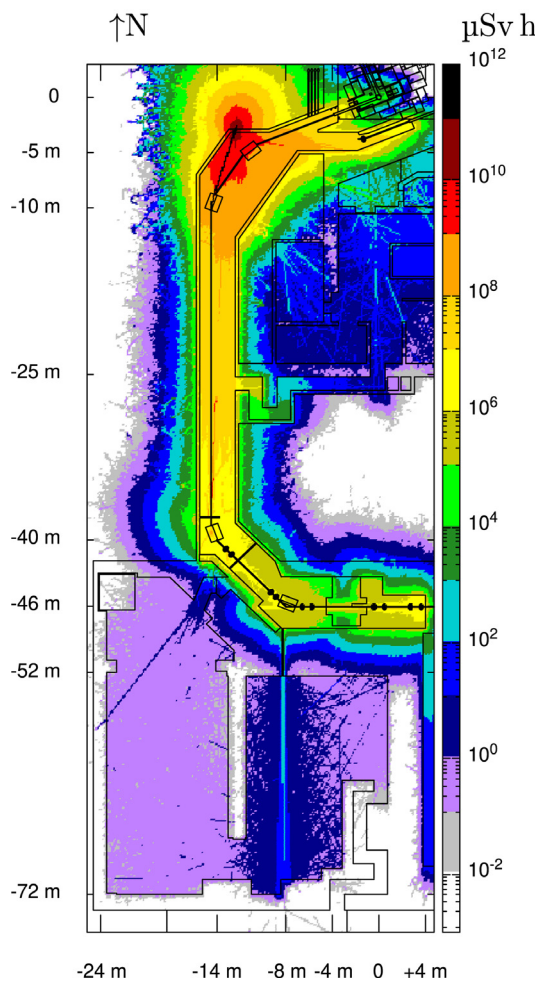


Fig. 8. Ambient dose rates, in $\mu\text{Sv h}^{-1}$, averaged over the tunnel height for the full beam loss corresponding to case 4.

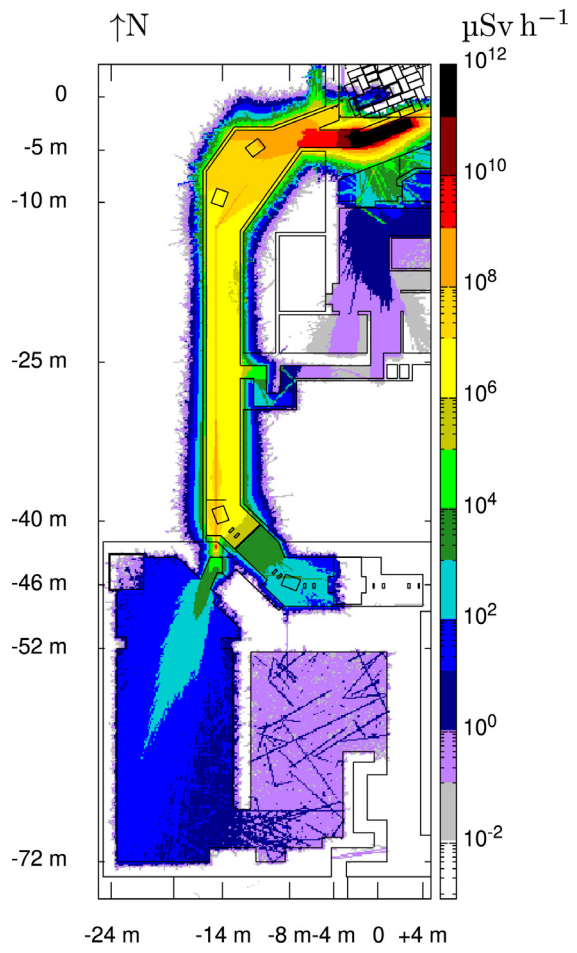


Fig. 9. Ambient dose rates, in $\mu\text{Sv h}^{-1}$, averaged over the tunnel height for the electron full beam loss (case 5) in the electron driver beam tunnel.

Table 1

Yearly average absorbed dose, assuming 5000 h of operation, in eleven detectors (Fig. 3), three dipoles and four quadrupoles (see Fig. 2). The sources of radiation considered were the chronic beam losses and the reflected shine from the target stations. The average distance between the detector and the beam line is also presented. The error in the values is within 3%.

Detector	\bar{D} [Gy y^{-1}]	$d_{(e)}$ [m]	$d_{(p)}$ [m]	Observations
D1G	620	.75	1.5	p-losses (41%); e-losses (59%)
D2C	416	2.25	1.4	p-losses (68%); e-losses (30%)
D3C	183	2.9	2.15	p-losses (54%); e-losses (46%)
D4C	1535	2.5	1.15	p-station (14%); e-losses (75%)
D5G	2418	1.5	1.25	p-station (9%); e-losses (86%)
D6C	1232	1.75	2.7	e-station (11%); e-losses (83%)
D7G	2437	1	2.65	e-station (5%); e-losses (89%)
D8C	7995	1.25	8.65	e-station (9%); e-losses (91%)
D9G	101	4.7	2.25	p-losses (~ 100%)
D10G	2.26E5	.6	1.6	e-losses (~ 100%)
D11C	874	2.2	1.45	p-losses (51%); e-losses (49%)
D1	2.07E4			p-losses (51%); e-losses (48%)
D2	2.17E4			p-losses (87%)
D3	3.32E4			p-losses (43%); p-station (45%)
Q1	5.68E5			e-losses (99%)
Q2	2.31E6			e-losses (~ 100%)
Q3	8.27E5			e-losses (~ 100%)
Q4	2.45E6			p-losses (44%); e-losses (56%)

a relatively low density the shine could more easily reach the ground level just outside of the main accelerator building (see Fig. 2). However, as per Fig. 10, the shine reaching the ground is well below 10 mSv h^{-1} .

As for the E-HALL, some radiation leaks through the doghouse opening, reaching close to 10 mSv h^{-1} in the E-HALL side. Presently, the services running next to the doghouse are not yet fully defined, and further work will be required to validate the shielding in this zone. Although in ideal ARIEL operation mode (*i.e.* simultaneous proton and electron beam delivery) the E-HALL should not be occupied, the presence of personnel in the E-HALL while the e-linac is off and during proton beam extraction is a likely scenario.

In case 3, a full beam loss takes place in the beam line pipe, upstream of the tunnel entrance maze (see Fig. 7-a). In earlier studies this was singled out as the worst catastrophic beam loss case for accessible areas of the B2 level [9]. Consequently, both shielding and a safety-critical monitor will be installed in between the tunnel and the hot-cells as denoted in Fig. 2. Above ground, as per Figs. 7-b and c, case 3 generates the highest ambient equivalent dose rates, standing generally above 10 mSv h^{-1} . Due to its effect at ground level potentially affecting the badge room, the ARIEL building and being at the very interface with the general public zone (see Fig. 2), it is paramount that the radiation monitoring system is able to trip the beam in the event of such a catastrophic beam loss. The locations deemed most relevant for this purpose were the southwest ARIEL rooms, both at tunnel and ground level, where radiation monitors can more effectively detect fields originating in the tunnel. Safety-critical monitors will be installed in those rooms as denoted in Fig. 2. In the unlikely event that a catastrophic beam loss occurs in that area, resulting in radiation levels of 50 mSv h^{-1} , the maximum dose accrued over the course of 250 ms is lower than $3.5 \mu\text{Sv}$.

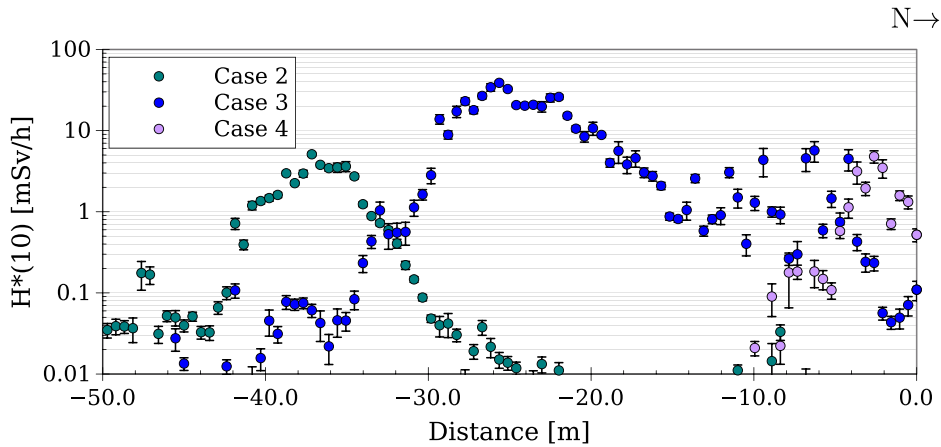


Fig. 10. Ambient dose rates above ground level, in mSv h^{-1} . The scored volume corresponds to a width of 1 m centered at the proton beam line ($E \leftrightarrow W$), a height of 1 m above ground level, and 50 m ($S \rightarrow N$) in steps of ~ 50 cm. Only the catastrophic cases 2, 3 and 4 were tallied since these are the major sources of radiation in the tunnel.

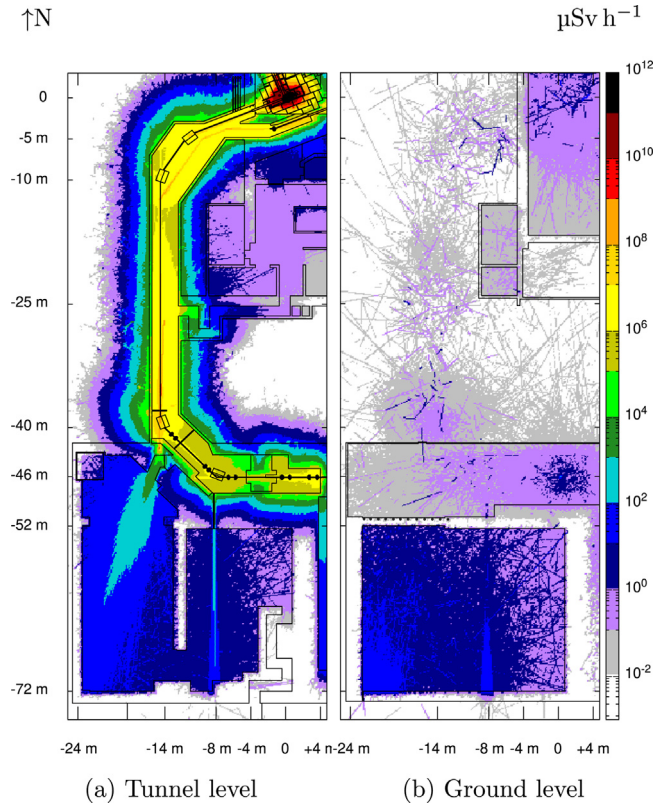


Fig. 11. Ambient dose rates, in $\mu\text{Sv h}^{-1}$, averaged over the tunnel height (a) and 2 m above ground level (b). The radiation from chronic beam losses is scored in combination with both target stations' irradiation.

As for case 4, the catastrophic loss occurs as a result of a malfunction of the magnet, causing the beam to be deflected to the tunnel wall (Fig. 8). Contrary to case 2, the ground level zone impacted includes a general public access area adjacent to the main administration building. Nevertheless the radiation level at the surface, as one can see in Fig. 10, ranges from $1\text{--}10 \text{ mSv h}^{-1}$ at the peak which is considerably lower than for case 3.

Regarding the last catastrophic event studied, it consists of an electron beam full loss in the last quadrupole before bending into the target station (Fig. 9). The main zone impacted is the Target Pit service room, which is not an accessible zone, but had its shielding recently reinforced because it is adjacent to the Hot-cell area that is regularly

occupied. It is clear in Fig. 9 that the shine reaching the hot-cell vicinity is negligible.

Chronic beam losses

Chronic beam losses, as depicted in Fig. 11 with the target stations' contribution, do not lead to dose rates above $1 \mu\text{Sv h}^{-1}$ in the hot-cell zone in the ARIEL facility. At ground level, in between the E-HALL and the ARIEL facility, it was found that dose levels were lower than $1 \mu\text{Sv h}^{-1}$. As for the background ambient dose rates inside the tunnel, they were generally close to 1 Sv h^{-1} and exceeded the tens of Sv h^{-1} when approaching the beam lines.

Regarding the absorbed dose rates quantified in Fig. 12, and despite a comparable maximum value for both beam lines, one can appreciate a clear difference between the spatial distribution of radiation perpendicularly from the beam axis. While the proton beam losses attain 1 Gy h^{-1} at ~ 25 cm the electron beam losses are shown to pose a higher risk as they descend to the same absorbed dose value at further distance from the beam between $1.25\text{--}1.5$ m (Fig. 12). This difference can be attributed to: the higher intensity of the electron beam loss when compared to its proton counterpart by a factor of 20; the large prevalence of forward-peaked electromagnetic radiation through a relatively long distance – stemming from *bremssstrahlung* in the beam pipe and air, as well as pair production processes and annihilation events – in the electron beam loss; and the relatively high predominance of highly ionizing electromagnetic radiation in the electron beam losses whereas the proton-induced mixed field has a dominant, more isotropic, neutron component.

Concerning the equipment damage in the tunnel, the radiation fields were characterized to provide ranges of radiation index (RI) [18] values, to help with selecting adequate materials and their location. The eleven detectors, during their lifetime of 30 years, sustain radiation levels that are compatible with a RI of 5 or less as per Table 1, except for “D8C” and “D10G”. The former is chiefly due to the shine resulting from the chronic electron beam losses in the rising track of the beam line, which incidentally impinges directly onto D8C at ceiling level. On the other hand, the absorbed dose in D10G surpasses an RI of 6.8 due to the electron beam losses' forward projected radiation stream being ‘trapped’ into an alcove created by the tunnel shine blocker just North of D1, the dipole and the walls of the tunnel (an effect visible in [-15:-38] of Fig. 11). Another contributing factor for these high radiation levels is the close proximity between the detector and the electron beam line, standing at a distance of 60 cm, as detailed in Table 1. In contrast, one should note the case of D1G, 30 m downstream of D1, positioned at a comparable distance to the beamline as D10G, which registers over 300 times less absorbed dose. This is due to the

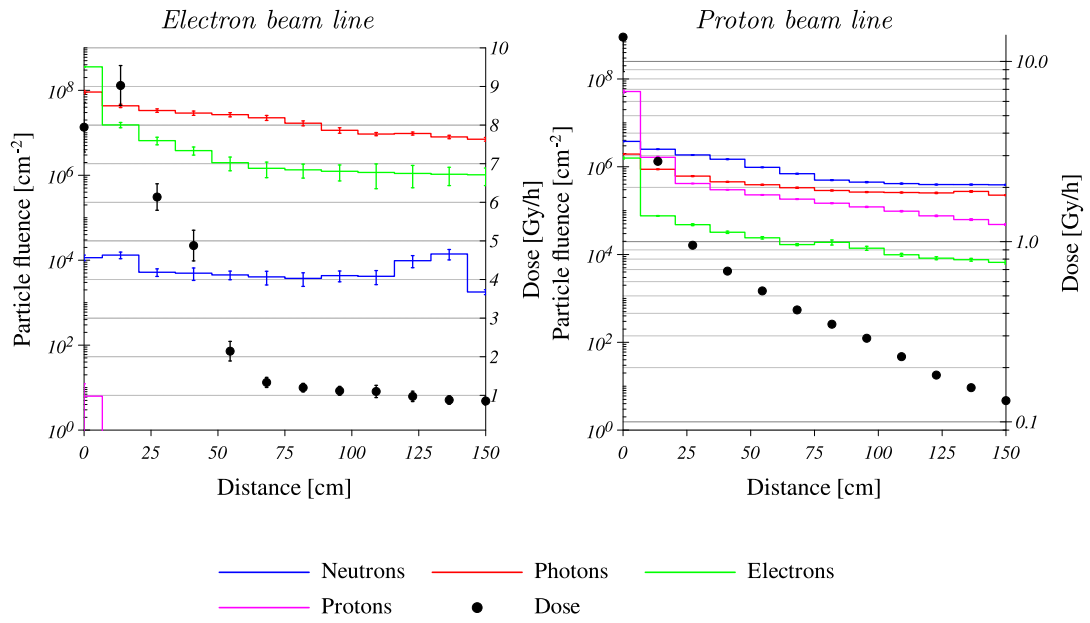


Fig. 12. Radiation fluence in cm^{-2} (lines) and Absorbed Dose in Gy h^{-1} (points) scored at 90° and up to a distance of 1.5 m from the beam line. The values are averaged over a 30 m extension, corresponding to the $[-40, -10]$ S-N section of the tunnel, and over 1 m centered at the respective beam line. These results are representative of chronic losses of each beam line only and thus do not include any target irradiation nor residual radiation contribution.

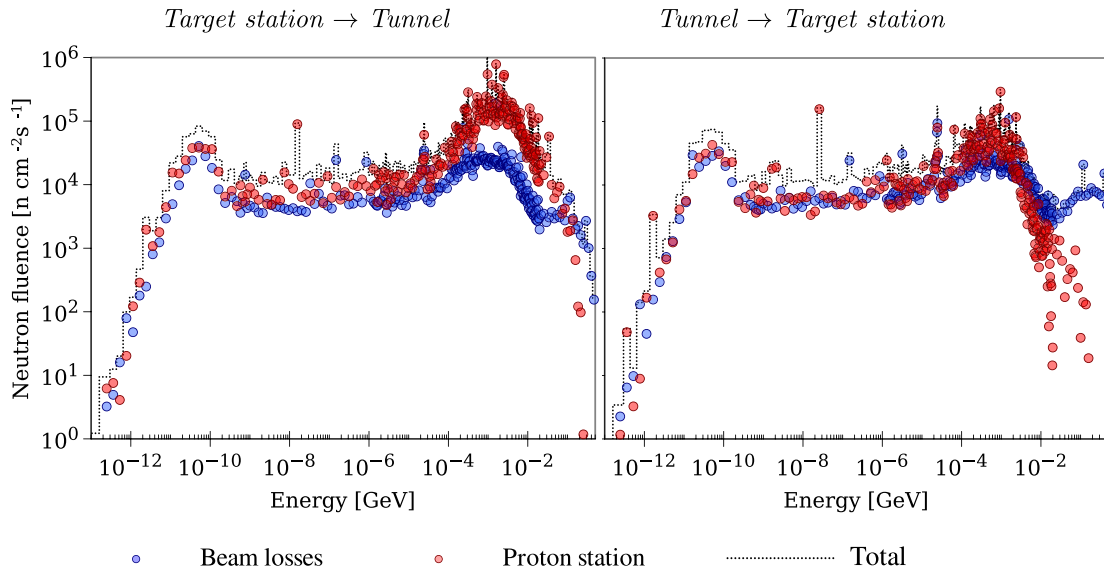


Fig. 13. Neutron fluence lethargy spectra in $\text{neutron cm}^{-2}\text{s}^{-1}$ originating from the chronic beam losses, proton and electron target stations (the latter included in the total). The values are scored in two directions, towards and exiting the target stations.

already mentioned tunnel shine blocker that contains a large portion of the forward projected shine, preventing it from reaching the northern part of the tunnel.

These results indicate that most services can be routed either close to the floor or at ceiling level using relatively common plastics, rubbers and adhesives [19,20]. However, materials employed closer to the beam line may accrue higher absorbed doses as shown with the data in Table 1, particularly for the dipoles and quadrupoles. In this case, for 30 years of operation, materials should have RI ranging from 5.8–7.8, which is beyond the dose limit for a large number of cable insulation materials ($2\text{-}5 \times 10^5 \text{ Gy}$) and could surpass pure epoxy resins ($2\text{-}5 \times 10^6 \text{ Gy}$) [21].

The values of absorbed dose scored in the detectors placed on dipoles D1–3 are within 21–33 kGy per year, requiring a minimum RI of 5.8 (Table 1) for 30 years operation. Considering that typically

the most radiation sensitive feature of these magnets is the electrical insulation [22] and the uncertainties inherent with the location of our detectors, the use of organic materials usage (e.g. epoxy resins) should be carefully weighted. For comparison, ARIEL dipoles in the target pit downstream from the target stations require the use of local shielding and radiation resistant CTD-101K resin to meet lifetime goals.

For the quadrupoles studied in Table 1, being placed along the electron beam line (see Fig. 2) they are therefore subject to higher dose rates (minimum RI of 7.2) as already detailed in this section. Q1 is the least affected. Although it receives direct shine from the electron target station the chronic loss component from the proton beam line is almost absent and the electron loss impinges onto the quadrupole not at a direct angle. Conversely, Q2–4 are unscathed by the reflected electron target station shine and, despite being directly exposed to the proton station driver beam opening, receive significant dose from losses in the main tunnel only.

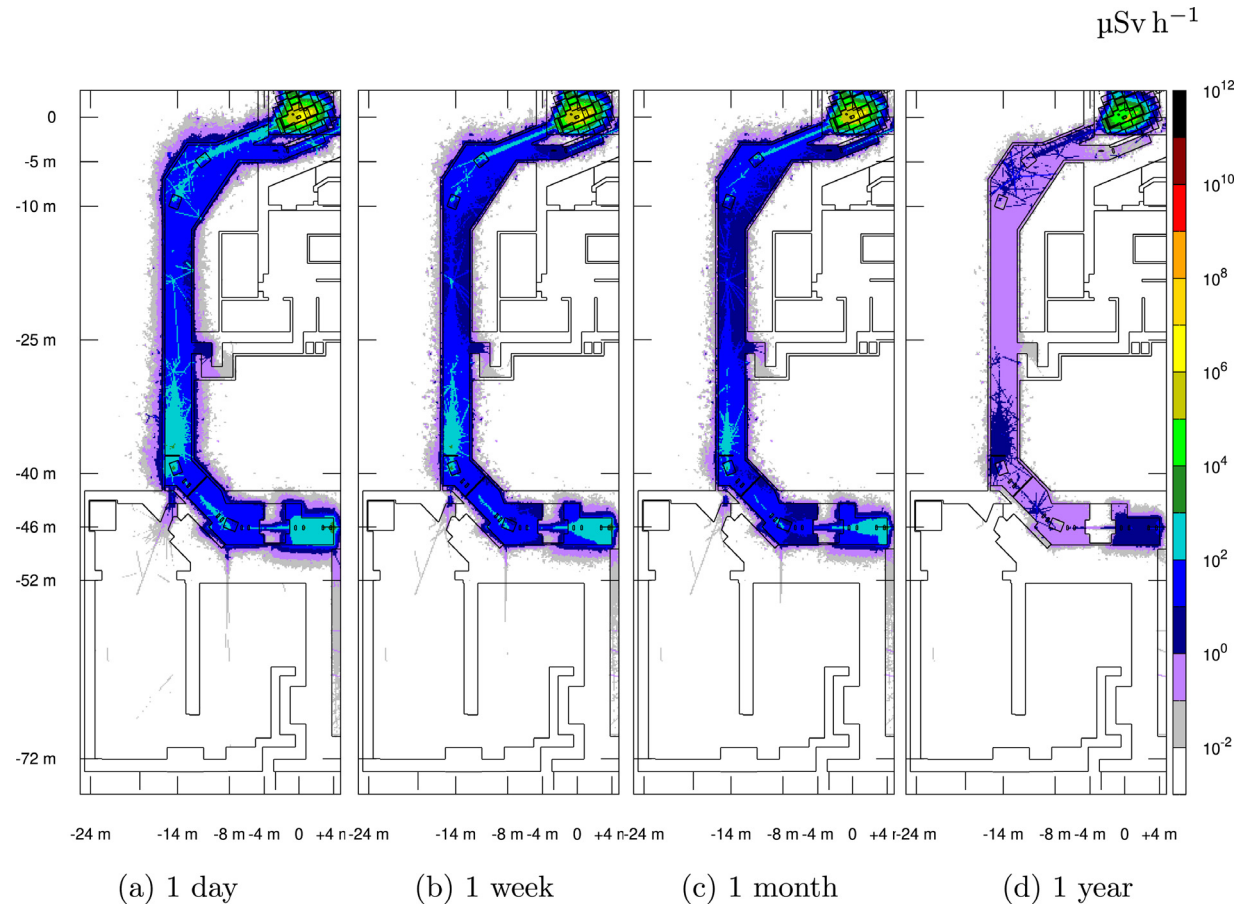


Fig. 14. Ambient dose rates at various times post-EOB assessed after 10 years of operation including the 3 month annual shutdown period. The result is averaged over a 2 m height above the tunnel floor and includes contributions from the electron or proton stations (without the respective targets).

The neutron fluence lethargy spectra were scored (see Fig. 13) at the interface between the main tunnel and both the proton and electron driver beam tunnels, denoted in figure's 3 top left view. This detector location was selected to score both a representative neutron fluence through the tunnel as well as the reflected neutrons from the proton target station. Note that the spectra in Fig. 13 correspond to values scored over a relatively large detector area but it is expected from the results in Fig. 12 that the neutron rates are highest near the proton beam line.

The direction of the fluxes, calculated towards the target stations and the tunnel, provides insight on the origin of the fluxes and could potentially help define an optimized shielding according to the direction of neutron incidence. The results in Fig. 13 indicate that the total neutron fluence are within the same order of magnitude for both directions and are generally driven by the neutrons originating in the proton target station and beam losses, making the effective application of localized shielding difficult.

A large quantity of neutrons, resulting from spallation and fission reactions in the ISOL target, exit the target station (red points) at energies above 10 MeV in the top left pane of Fig. 13 whereas the right pane lacks this higher energy neutron component. The few proton-associated higher energy neutrons scored result from back-scattered neutrons in the tunnel walls and magnets. A different effect can be observed in the case of the chronic beam losses, with neutrons with energy higher than 100 MeV directed towards rather than away from the stations.

Regarding the electron station, it plays but a minor role not only because the neutron production in the electron targets is limited (mostly resulting from photonuclear interactions and photofission in fissile targets) but also because of the additional scattering undergone by

neutrons in the electron driver beam tunnel's southern wall before reaching the detector.

Personnel access scenarios

Maintenance in the tunnel post-EOB is likely to take place during the yearly shutdown which lasts typically about 3 months. However, the variation in residual dose rates, as per Fig. 14-(a,b,c), is relatively small up to 1 month post EOB. Until this time, dose rates are generally lower than 100 $\mu\text{Sv h}^{-1}$ in most of the tunnel, with hotspots exceeding 100 $\mu\text{Sv h}^{-1}$ in some regions of the beam line including the collimator and the dipoles. This is largely due to proton induced activation from spallation or neutron capture interactions generating isotopes of Co, Mn and Fe in beamline components, while the electron beam contributes but marginally to the activation inventory. These residual dose rates can be regarded as baseline values since the presence of additional structures and material choice might increase the levels of radiation throughout the tunnel. Further validation should therefore be performed with an as-built model.

The other main contribution to the residual dose rates in the tunnel are the activated target stations. Based on this works' results, provisions will be made to install localized shielding to mitigate shine from the target stations into the tunnel. The need for localized shielding at hot spots is assessed with a survey at the time an area is opened for access. As for the 1 year post EOB scenario in Fig. 14-d, representative of a longer shutdown period which is expected every 10–15 years, the residual dose rates are within 1–10 $\mu\text{Sv h}^{-1}$. The long term background residual dose rates at one year post-EOB is largely driven by ^{54}Mn , ^{56}Co and ^{46}Sc .

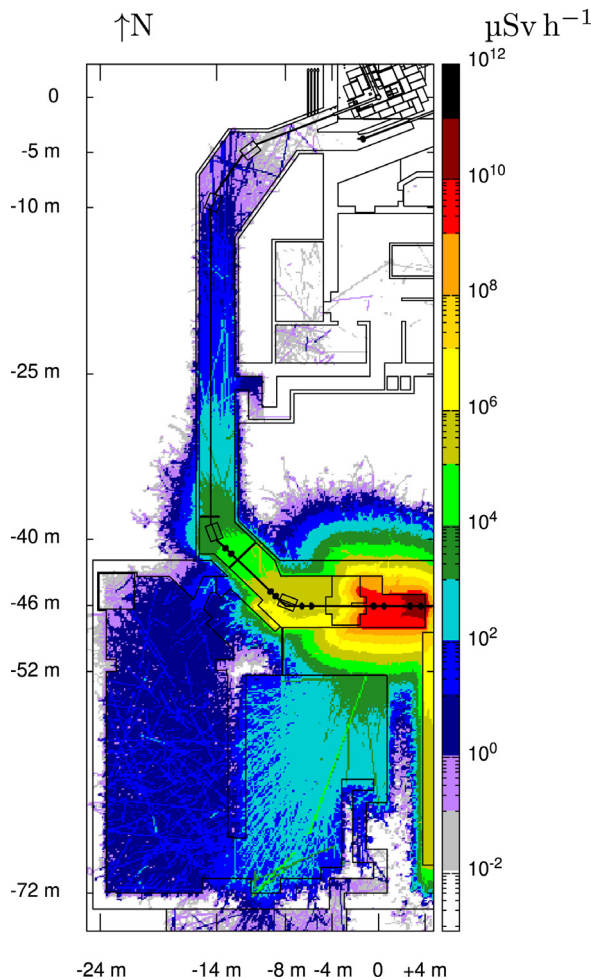


Fig. 15. Ambient dose rates, in $\mu\text{Sv h}^{-1}$, averaged over the tunnel height during a full beam loss originating from the main cyclotron.

Regarding the shine from a full beam loss from the cyclotron at the entrance of the “Pharaoh’s tomb”, depicted in Fig. 15, it is evident that prompt dose rates largely surpass the residual fields. This is an extremely unlikely and conservative scenario. However, even in such case, the combined effect of the collimator shielding and the shielded door downstream (between the proton cave and the northbound section of the tunnel) can attenuate prompt fields to 10 mSv h^{-1} . These radiation levels are temporary as there are numerous beamspill monitors continuously operating in the cyclotron vault that warn the Control Room and can shut off the cyclotron if predetermined radiation levels are reached. Nevertheless, apart from the shine originating in the small opening of the collimator, the latter efficiently attenuates the main radiation cascade by almost 5 orders of magnitude and thereupon its design can be deemed adequate. Furthermore, in view of the lack of radiation monitors inside the tunnel, it was decided to reinforce the shielding door and move it upstream to ensure the tunnel area are closer to the residual background in the event of a full beam loss from the cyclotron.

5. Conclusion

This study assessed the impact of the beam losses in TRIUMF’s BL4N Proton cave and ARIEL tunnel during electron and proton beam operation.

Despite catastrophic beam losses having a limited impact in the ARIEL facility, restricted to case 3 in which shine bypassed the tunnel

maze, the effects at ground level are more significant (case 2–4). Although a few locations have a peak dose rate approaching the 50 mSv h^{-1} averaged over 50 cm they are always within the limit, and these also have a safety factor of three built in. In the E-HALL and main accelerator building considerable leakage was observed (cases 0 and 1), due to the present service chases configuration, which will have to be either optimized or shielded. Moreover, further studies will focus on the shine leaking through the doghouse into the E-HALL using proton maximum credible incidents (case 2). The existing network of radiation monitors will be extended to promptly trip the beam when excursions above background are detected.

The tunnel design and shielding proved to be effective in attenuating the prompt ambient dose rates in the ARIEL facility. A more detailed analysis of the chronic beam losses indicated that despite the fact that proton beam losses drive the shielding design, the electron beam losses can dominate the absorbed dose rate fields in the tunnel. Consequently, the combined effect of the losses in the proton and electron beam lines can require, particularly closer to the latter, radiation hardened components in order to meet operational lifetime goals. On the other hand, it has been found that neutron fluences at the northern limit of the main tunnel were driven by a combination of proton target station and proton chronic beam losses.

This study also showed that the residual dose rate levels in the tunnel after 10 years of operation were sufficiently low to allow for temporary access during an yearly shutdown, with an unshielded background close to $100 \mu\text{Sv h}^{-1}$. Depending on the nature of the maintenance work, local shielding might be necessary. Also, restrictions pertaining to the access to specific areas and allotted time will have to be enforced based on the extant radiation fields (a radiological survey will be conducted prior to each access). After one year, a situation representative of a long shutdown, ambient residual dose rates were lower than $10 \mu\text{Sv h}^{-1}$. To mitigate the overall dose accrued, less pressing tasks will likely be performed closer to the end of the shutdown, and start in the zones where the radiation levels are lower.

Moreover, the collimator shielding design was validated against a full beam loss from the main cyclotron during the (unlikely) human presence in the tunnel. The ambient dose rates in the main tunnel were attenuated to less than 10 mSv h^{-1} providing sufficient margin of safety until the beam is tripped.

Declaration of competing interest

The authors declare that they have no known competing financial interests or personal relationships that could have appeared to influence the work reported in this paper.

Data availability

Data will be made available on request.

Acknowledgments

The authors wish to acknowledge the ARIEL teams for the information provided, Kel Raywood for technical assistance and EH&S for providing the computational resources through TRCOMP. ARIEL is funded by the Canada Foundation for Innovation, the provinces of AB, BC, MB, ON, QC, and TRIUMF. TRIUMF receives federal funding via a contribution agreement with the National Research Council of Canada.

References

- [1] R. Laxdal, The proposed ISAC-III (ARIEL) low-energy area and accelerator upgrades, in: Proceedings of LINAC08, Victoria, BC, Canada, 2008.
- [2] L. Merminga, et al., ARIEL: TRIUMF’s advanced rare isotope laboratory, in: Proc. IPAC 2011 (1917–1919), 2011.
- [3] J. Bagger, et al., TRIUMF in the ARIEL era, IPAC (2018).
- [4] T. Planche, et al., Commissioning and early operation of the ARIEL e-linac, in: Proceedings of LINAC2016, East Lansing, MI, USA, MO2A03, 2016.

- [5] Y. Rao, et al., New proton driver beamline design for the ARIEL project at TRIUMF, in: IPAC2018, Vancouver, BC, Canada, 2018.
- [6] F.W. Jones, et al., Simulation study of halo collimation in the TRIUMF ARIEL proton beam line, in: Proceedings of IPAC2017, Copenhagen, Denmark, 2017.
- [7] M. Alcorta, et al., Commissioning of the ARIEL E-LINAC Beam Loss Monitor System, in: International Beam Instrumentation Conference (8th), Malmö, Sweden, 2019.
- [8] A. Trudel, et al., Design of a compact shielding envelope and elements of radiological protection at the TRIUMF-ARIEL facility, *Rad. Phys. Chem.* 170 (2020) 108640.
- [9] R.S. Augusto, et al., An overview of the shielding optimization studies for the TRIUMF-ARIEL facility, *Nucl. Instrum. Methods Phys. Res. A* 1005 (2021) 165401.
- [10] L. Moritz, J. Drozdoff, G. Dutto, F. Mammarella, M. Mouat, R. Ruegg, Safety critical monitoring for prompt radiation hazards, in: Proceedings of the 2003 Particle Accelerator Conference, vol. 1, 2003, pp. 638–640, <http://dx.doi.org/10.1109/PAC.2003.1288997>.
- [11] A. Trudel, TRIUMF safety report, 2011.
- [12] A. Fassò, A. Ferrari, J. Ranft, FLUKA: a multi-particle transport code, 2005, CERN-2005-10, INFN/TC 05/11, SLAC-R-773.
- [13] T.T. Böhnen, et al., The FLUKA code: Developments and challenges for high energy and medical applications, *Nuclear Data Sheets* 120 (2014) 211–214.
- [14] V. VLACHOURIS, FLAIR: A powerful but user friendly graphical interface for FLUKA, in: Proc. Int. Conf. on Mathematics, Computational Methods & Reactor Physics (M&C 2009), Saratoga Springs, New York, 2009.
- [15] M. Pelliccioni, et al., Overview of fluence-to-effective dose and fluence-to-ambient dose equivalent conversion coefficients for high energy radiation calculated using the FLUKA code, *Rad. Prot. Dos.* 88 (4) (2000) 279–297.
- [16] H. Sorge, H. Stoecker, W. Greiner, Poincaré invariant Hamiltonian dynamics: Modeling multi-hadronic interactions in a phase space approach, *Ann. Physics* 192 (266) (1989).
- [17] Inc. Composite Technology Development, Ctd-101k epoxy resin system, 2021, https://Ncsx.Ppl.Gov/NCSX_Engineering/Materials/InsulationProperties/CTD-101K_Datasheet_2003.Pdf, (accessed on 16 July 2021).
- [18] IEC 60544-4, Electrical insulating materials - determination of the effects of ionizing radiation - Part 4: Classification system for service in radiation environments, 2003, Ed. 2.0 b.
- [19] M. Tavlet, H. Schönbacher, Compilation of radiation damage test data - part I, CERN-89-12, 1989.
- [20] M. Tavlet, A. Fontaine, H. Schönbacher, Compilation of radiation damage test data - part II, CERN 98-01, 1998.
- [21] H. Schönbacher, M. Tavlet, Absorbed doses and radiation damage during the 11 years of LEP operation, CERN-TIS2002-010-DI-PP, 2002.
- [22] A.F. Zeller, J.C. DeKamp, Radiation resistant magnet R&D at the NSCL, in: Proceedings of the 2003 Particle Accelerator Conference, 2003.